2023 IEEE/ASME International Conference on Advanced Intelligent Mechatronics (AIM)
June 28-30, 2023. Seattle, Washington, USA

# Design and Control of a Ground-Aerial Dual Actuator Monocopter (G-ADAM)

Brian Leonard Suhadi, Timothy Wong Zhi Heng, Shane Kyi Hla Win, Luke Soe Thura Win and Shaohui Foong

***Abstract*—The monocopter's distinctive single-wing design, which mimics an autorotating samara seed, has sparked substantial interest in expanding its versatility for various applications. In this regards, the Ground-Aerial Dual Actuator Monocopter (G-ADAM) – a hybrid multi-modal monocopter capable of transforming from flying to ground movement, and vice versa – addresses the latest trend of transformable robots that can operate in diverse environments. With only two actuators, G-ADAM can promptly transition between ground mode and aerial mode in just approximately 3 seconds. The motor used for the aerial mode is also utilized as propulsion for the ground mode, while the steering mechanism, controlled by a servo through physical linkages, provides control over the direction of the motor thrust in ground mode. A closed-loop control with manual tuning is applied to enable autonomous operation and position control during aerial and ground missions. Overall, G-ADAM successfully demonstrates the capability to operate and transition between ground and aerial modes.**

***Index Terms*—Monocopter, roadable aircraft, transformable robot, multi actuator, ground aerial robot**

## I. INTRODUCTION

In the last decade, the development of Unmanned Aerial Vehicles (UAVs) and Unmanned Ground Vehicles (UGVs) have been significantly evolving with the advancement of technologies [1]. The integration of both types of unmanned vehicles has begun to unlock new possibilities for versatile applications. A UAV has the advantage in terms of providing fast traveling time from one location to another while a UGV has the capability to support heavier payload and longer missions [2]. The integration can be classified into two main aspects: collaboration and cooperation between UAV and UGV, and a unified platform that integrates both types of vehicle capability. For instance, Hament and Oh [3] developed a team of autonomous UAVs and UGVs to inspect civil infrastructure. The robotic collaboration system consists of a UAV that generates an augmented map, and transports and deploys a UGV equipped with sensors and nondestructive testing to improve the map further.

For the second aspect, there is a growing interest to combine both types of vehicles into a single platform. Fusing both UAV and UGV into a single platform is a challenge due to their distinct design principles. Recently, there has been a significant attempt to develop such a platform by Kalantari et al. [4] that combines aerial and ground vehicles into a single platform. The design, which has the purpose of long-endurance missions, is developed from a quadrotor configuration with additional brushed DC motors to drive the four platform wheels independently. Another hybrid robot with multi-modal locomotions is introduced by Nir and David [5] that integrates a quadcopter with a four-wheeler vehicle function, called the flying STAR. When the robot is on the ground, it can transform from a quadcopter arrangement into a UGV by sprawling its four legs up and down. It is also equipped with step-up gearboxes that translate the motor rotation into wheel rotation, thus providing forward thrust for the robot while on the ground.

Another research by Tanaka et al. [6] developed a smaller version of the hybrid robot for deployment in the disaster area. It utilizes a small quadcopter design that is equipped with two active wheels and a passive wheel to drive through terrains and stabilize orientation respectively. Mulgaonkar et al. [7] also introduced the smallest quadrotor, called the flying monkey, which is equipped with walking and gripping capabilities. Another unique hybrid ground-aerial robot developed by Daler et al. [8] presented a tail-sitter drone that is capable of walking by using its wings.

Overall, most hybrid ground-aerial vehicle designs are mainly based on quadrotor and tail-sitter configurations. One area of UAVs that has not been explored for multi-modal locomotion is the monocopter. It has seen an increase in research that introduces multiple functions, control methodologies, and designs. The monocopter is inspired by a phenomenon of a falling samara seed that autorotates upon descent to decelerate and disperse for reproduction [9], [10]. Luke et al. [11] had successfully produced a controllable monocopter with a single actuator called Single Actuator Monocopter (SAM). The design of SAM is one of the most optimum monocopter designs that can be extended into a variety of applications and modifications.

Amongst various possibilities for developing a new kind of monocopter, one riveting area of research in monocopter focuses on enhancing its capability to transform into a different type of vehicle or mode of operation with multiple functions allowing the drone to develop a more versatile deployment. For instance, Transformable HOvering Rotorcraft (THOR) by Low et al. [12] had been developed as a monocopter that can transform into a bi-copter and tail-sitter drone. Besides autorotating, THOR is capable to fly and hover vertically with only two motors and also, cruising horizontally like a fixed-wing aircraft enhancing its capability to fly over long distances.

The two-flight mode capable single-wing rotorcraft with mid-air transition ability, developed by Hitesh et al. [13], is another example of a transformable monocopter. Cai et al.

The authors are with Engineering Product Development Pillar, Singapore University of Technology & Design (SUTD), 8 Somapah Road, Singapore 487372. (Corresponding e-mail: foongshaohui@sutd.edu.sg)

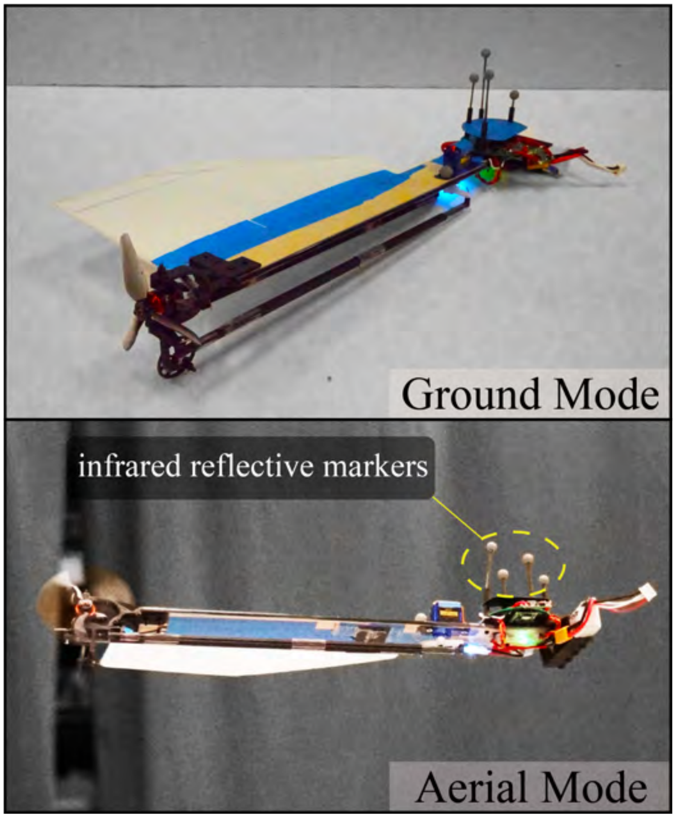


Fig. 1. G-ADAM is a monocopter that aims to realize a transformable UAV-UGV robot with a minimal number of actuators. The upper and lower pictures show G-ADAM in the ground and aerial modes, respectively.

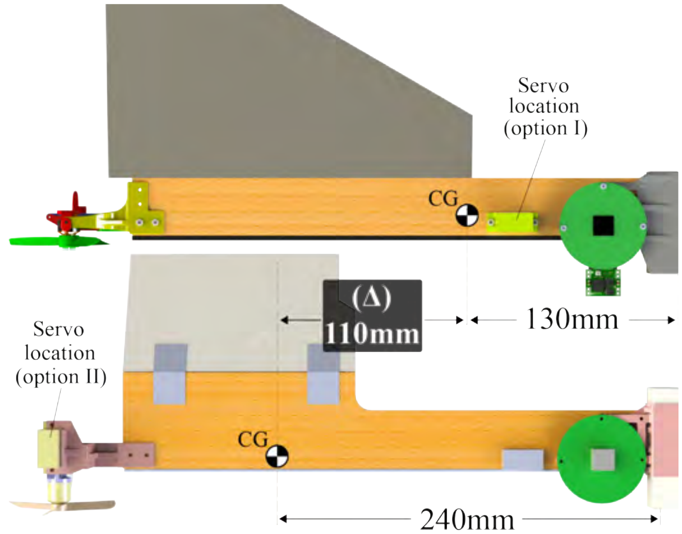


Fig. 2. Two mounting locations of servo are considered. If the servo is mounted directly on the motor's vertical axis at the wingtip, the Center of Gravity (CG) is shifted by 110mm.

[14] had also developed a Modular Single Actuator Monocopter (M-SAM) that can passively separate into two modular monocopters in mid-air to fly cooperatively. Furthermore, Cai et al. [15] explored the area of modular wings and control modules for multi-wing monocopter that can be reassembled into different configurations to enhance modularity and performance. As the development of monocopters continues to evolve, incorporating other functions of different types of vehicles such as Unmanned Ground Vehicles (UGV), Unmanned Surface Vehicles (USV), and Underwater Unmanned Vehicles (UUV) seems only natural. Therefore, in this paper, we present the first transformable monocopter that can function both as a UAV and UGV. The contributions of this work are as follows:

- Our proposed transformable monocopter design concept, as shown in Fig. 1, allows the robot to operate both in the air and on the ground using a single platform. The design only utilizes two actuators to enable both aerial and ground functions
- We have built a prototype based on the new concept design, which we have named the Ground-Aerial Dual Actuator Monocopter (G-ADAM). To evaluate the performance of the robot in terms of transforming functionality and operations in both air and ground modes, we conducted experiments using closed-loop and manual control.

## II. Design Concept and Analysis

This section introduces the design concept of G-ADAM to highlight design considerations and feasibility. The capability of G-ADAM is divided into two main modes: ground mode and aerial mode. In the ground mode, the propulsion and steering mechanism are presented. Furthermore, in aerial mode, the methodology of control is discussed.

### A. Design Concept

The primary focus in designing G-ADAM is to achieve dual functions that allow flying in the air and moving on the ground with minimal actuators. Fundamentally, G-ADAM implements the design of SAM by Luke et al [11] since its design has been optimized through iterations of simulations. However, with the SAM design, the motor only enables propulsion and pitch-roll control airborne. An additional mechanism is required to enable steering for directional control while the robot moves on the ground. For the approach to this issue, we study an airboat [16] – a watercraft that utilizes an aircraft-type propeller powered by an aircraft engine for propulsion on the water – and a bicycle steering mechanism [17]. The airboat utilizes the power of motor-propeller configuration to produce thrust on the water. It also has a secondary rudder actuator that diverts the rearward air generated by the propeller thrust. Thus, this allows a yaw motion for the vehicle to turn left or right. However, a secondary rudder alone for G-ADAM is not sufficient to transition into ground mode. In terms of feasibility, following a bicycle steering mechanism is more practical to allow ease of transitioning between the ground and aerial modes.

Hence, G-ADAM incorporates an additional actuator, a servo, to allow control over the thrust direction generated by the motor. The motor is mounted on the motor mount holder which allows rotation around its vertical axis. There are two

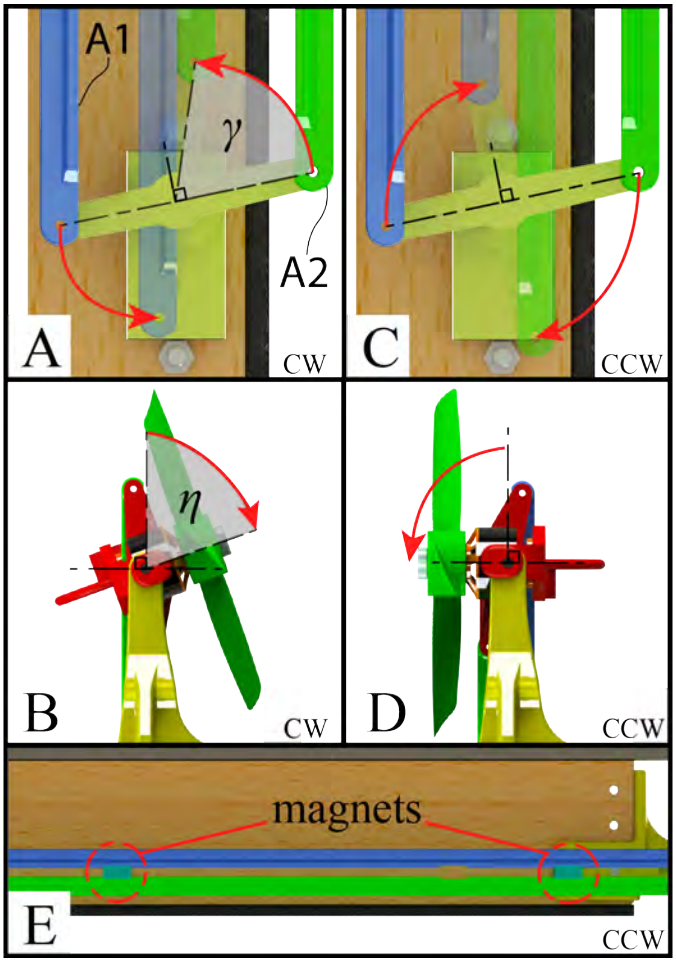


Fig. 3. Steering mechanism for ground mode is controlled by a servo actuator. In A, the servo angle $\gamma$ is the angular displacement by the rotation of the servo arm. In B, the steering angle $\eta$ is the angular displacement by the rotation of the motor mount - motor configuration. The total turning angle is 160$^{o}$ with 70$^{o}$ in clockwise (CW) direction shown in A and B, and 90$^{o}$ in counter-clockwise (CCW) direction shown in C and D. The CCW position shown in C and D is also used in aerial mode. In the aerial mode, two pairs of magnets attract and retain the two linkages A1 and A2.

main considerations for the location of the servo to enable steering control as shown in Fig. 2. For the first consideration, the servo is placed nearer to the main body where the CG is located. However, extended linkages are needed to translate the servo rotational motion to the motor mount to control the thrust direction. Thus, this design adds additional components, and possibly, is heavier.

For the second option, the servo is placed directly at the wing tip on top of the motor which acts as a hinge. This design does not require extended linkage and thus, it is lightweight and has more rotational freedom since both actuators are aligned on the same z-axis. However, placing an additional actuator at the wing tip disrupts the weight distribution for optimal flight performance since the Centre of Gravity (CG) is shifted towards the motor side by 110mm as shown in Fig. 2. Furthermore, the servo body also obstructs the area where the thrust is generated by the motor, which hinders the robot from harnessing the thrust optimally. From these two considerations, the first option, even though possibly heavier, is chosen since it provides better weight distribution and is able to maximize the thrust generated by the motor.

### B. Ground Mode

The steering mechanism is mainly controlled by a servo that is connected to the motor mount via two 3D-printed linkages, link A1 and A2 as shown in Fig. 3.A. In Fig. 3, the mechanism is explained to have bidirectional rotation: clockwise (CW) and counter-clockwise (CCW). The servo angle and the steering angle are denoted by $\gamma$ and $\eta$. For the robot to turn right, the servo has to rotate in the CW direction as shown in Fig. 3.A. and this translates into the motor rotating in the CW direction as shown in Fig. 3.B.

On the other hand, the robot turns left if the servo rotates in the CCW direction as shown in Fig. 3.C., which translates into the motor rotating in the same direction as shown in Fig. 3.D. Due to the rotational limitations of the servo, the maximum achievable rotational angle is 160$^{o}$. In this prototype, the maximum $\eta$ is divided into 70$^{o}$ in the CW direction and 90$^{o}$ in the CCW direction, with the latter required to support an optimum flight operation in aerial mode. The steering mechanism coincides with the center of gravity axis to minimize the torque produced by the centrifugal force.

G-ADAM primarily uses the steering mechanism in ground mode to control yaw direction to the left and right while propelling forward. The relationship between the steering angle and the servo angle is further analyzed using the SolidWorks Motion Study Analysis. The maximum derivative of the graph representing the steering angle as a function of the servo angle is obtained at zero steering angle as follows:

$$\Delta\eta = 1.015\Delta\gamma \tag{1}$$

When the maximum steering angle is reached, the derivative of eq.(1) turns zero. This signifies that the steering mechanism has entered the locking mechanism mode. The locking mechanism is a critical function for the aerial mode since it reduces the load on the servo to provide sufficient torque against the centrifugal force due to the body rotation.

### C. Aerial Mode

In aerial mode, G-ADAM operates as a monocopter. Research by Luke et al. [10] found that a monocopter is able to fly with a single actuator through the use of cyclic control. The cyclic control in G-ADAM performs similarly by rapidly increasing and decreasing lift force at different areas of rotation by changing the motor thrust. This approach can be achieved by using cyclic square waves that allow continuous rapid changing of the motor thrust. This mechanism allows G-ADAM to perform pitch and roll by increasing thrust at one region and decreasing thrust at the remainder or opposite region. The difference in the lift between the two regions creates an imbalance, resulting in lateral and longitudinal motion. Increasing and decreasing the motor thrust without

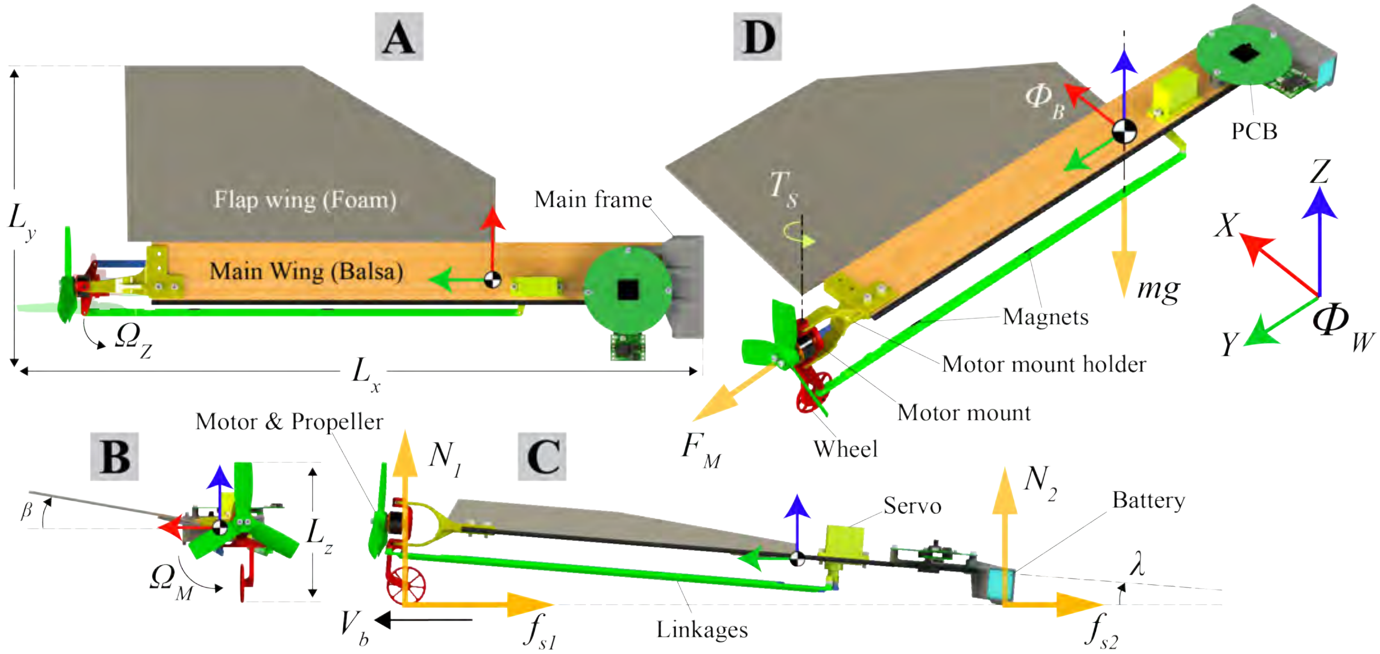


Fig. 4. (A), (B), and (C) are top, front, and side views of G-ADAM respectively. (D) shows the isometric view of G-ADAM with $\Phi_{\mathbf{W}}$ *(X, Y, Z)* as the world frame and $\Phi_{\mathbf{B}}$ as the body frame at the center of gravity with its axes aligned to $\Phi_{\mathbf{W}}$. Linear velocity $V_B$ in ground mode and rotational velocity $\Omega_{\mathbf{Z}}$ in aerial mode are measured with respect to $\Phi_{\mathbf{W}}$ and $\Phi_{\mathbf{B}}$ respectively. $\Omega_{\mathbf{M}}$ is the propeller's direction. $L_x$, $L_y$ and $L_z$ are the overall dimensions while Band $\Delta$are the flap wing trailing edge angle and elevation angle with respect to the ground respectively. $F_M$ and $F_g$ are the force produced from the thrust of the motor and the gravitation force. $f_{s1}$ and $f_{s2}$ are the friction forces that resist motion at the wheel and the main frame. $N_1$, and $N_2$ are normal forces acting at the point of contact between G-ADAM body and the ground. $T_S$ is the torque produced by the servo.

cyclic control allow the robot to rotate faster and slower, resulting in climbing and descending motion respectively.

The square waves cyclic control for the motor can be applied as follows:

$$F_{\text{amp}} = k\sqrt{\text{pitch}^2 + \text{roll}^2} \tag{2}$$

$$\zeta_{\text{c}} = \text{atan2}(\frac{\text{pitch}}{\text{roll}}) \tag{3}$$

Where $F_{amp}$ and $\zeta_c$ are the amplitude thrust and directional control of the input pitch and roll respectively, while $k$ is a constant to scale the effectiveness of roll and pitch input. By using Eq.(1) and Eq.(2), the cyclic thrust, $F_{cyclic}$, can be defined as,

$$F_{\text{cyclic}} = \begin{cases} F_{\text{o}} + F_{\text{amp}} & \text{if } \sin(\zeta_{\text{z}} + \zeta_{\text{c}} + \zeta_{\text{off}}) > \epsilon \\ F_{\text{o}} - F_{\text{amp}} & \text{otherwise} \end{cases} \tag{4}$$

where $\zeta_z$ and $\zeta_{off}$ are the current azimuth heading of the robot and an offset angle for correction due to gyroscopic precession and other factors.

## III. Prototyping and Experiment Setup

This section presents the prototyping process with each subsection discussing the details regarding the electronics components, actuation, and manufacturing methodologies used in creating the prototype. Additionally, the experimental setup is discussed.

TABLE I
G-ADAM Design Parameters

| Parameter | Value | Unit |
|---|---|---|
| $m$ | 144 | g |
| $L_x$ | 423 | mm |
| $L_y$ | 183 | mm |
| $L_z$ | 89 | mm |
| $\beta$ | -0.18 | rad |
| $\lambda$ | 0.08 | rad |

### A. Electronics and Actuation

The main component of G-ADAM is situated on the Printed Circuit Board (PCB) as shown in Fig. 4.D. which is designed to provide structural integrity and ease of wiring and electronics mounting. The design features a microcontroller Teensy 3.2 (PJRPC), a step-down 5 V regulator, a 3-axis magnetometer (PNI RM3100), a F35A 32-bit Electronic Speed Control (ESC) (T-Motor), and two micro receivers D8 (FrSky) as shown in Fig. 4.C and D. The actuation comprises two components: a motor F15/KV6000 equipped with HQProp propellers (T3x2.5x3 CCW) and a digital micro servo Tower Pro™ SG90. Two long flex PCBs are used to connect the two actuators to the microcontroller.

### B. Manufacturing Prototype

G-ADAM weighs 144 grams, and other relevant parameters are presented in Table 1. To facilitate component replacement, most of the G-ADAM components are designed to be easy to fabricate and replace. We use Fused Deposition Modelling (FDM) 3D printing to manufacture several components, including the PCB and battery housing, servo-to-motor linkages, motor mount, motor mount holder, wheel, and flap holder. Markforged Mark Two 3D printer and Onyx filament material are used. The printing is set with an accuracy of 0.1mm, and the material is selected for its strength and ability to absorb impact.

The main wing and flap shown in Fig. 4.A. are produced using balsa wood with a thickness of 2mm and foam with a thickness of 2.5mm, fabricated with a laser cutter Lionsforge Craftlaser. The lateral strength of the balsa wood at the servo location is too weak to sustain the weight and actuation movement of the servo mounted on it. Hence, two approaches are applied in this prototype. Firstly, two pieces of carbon fiber sheets with 0.8mm thickness are glued to the critical mounting points along the balsa wing at the servo joints. This provides enhanced lateral strength and minimizes wing twists due to the weight of the mounted components. Secondly, the balsa wing and the carbon fiber sheets are laminated together with 120μm laminating film for overall rigidity. This provides the wing with sufficient longitudinal and lateral strength to minimize undesired flex, twist, and any other tear due to aerodynamic and centrifugal forces generated during a flight in a high rotating motion.

### C. Experiment Setup

The experiment was conducted in a drone flying area with a size of 7m(length) x 5m(width) x 2.3m(height). A total of eight motion-captured cameras, OptiTrack Prime 41, were installed around the area. As shown in Fig. 1, five infrared reflective markers were placed on G-ADAM to enable camera tracking and real-time generation of position and orientation data. This data was processed via MATLAB with a closed-loop control running. The control produced an output in the form of pwm signal that is transmitted via a Radio Control (RC) module and received by the onboard drone receiver.

For safety, the second onboard receiver was used to allow the pilot, who was present in every experiment, to take control of the drone in case of any potential collision or dangerous behavior. The control methodology of G-ADAM followed the control used in the first foldable single-actuator rotary wing micro aerial vehicle, as discussed and tested in [18].

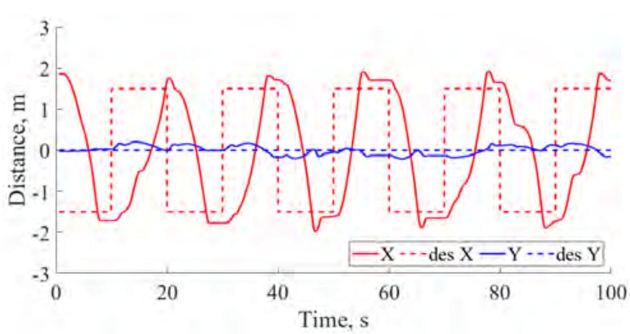


Fig. 5. Experiment I performance: X and Y coordinates between the actual and desired path against time.

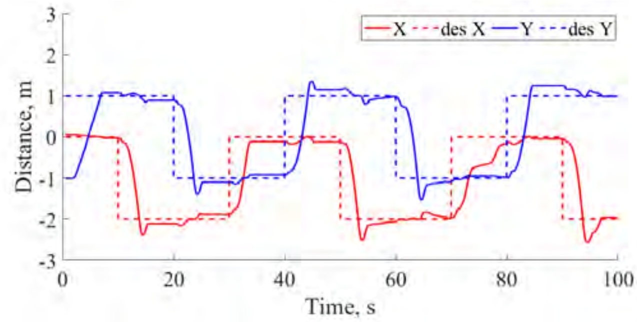


Fig. 6. Experiment II performance: X and Y coordinates between the actual and desired path against time.

## IV. Experiment and Performance Analysis

This section presents the experimental evaluation of the three main modes: ground mode, aerial mode, and transition between ground and aerial mode. The experiment results are subsequently analyzed and discussed.

### A. Ground Mode Test

Three experiments were conducted to assess the performance of G-ADAM in ground mode operation with the closed-loop controller. In Experiment I, the robot was commanded to move bidirectionally between two waypoints: (1.5,0,0), and (-1.5,0,0) for five consecutive runs. As shown in Fig. 5, G-ADAM relatively achieves position control in X and Y directions. Slightly higher mean and std in position error are observed at 1.58m and 1.16 respectively as shown in Table II. The robot traveled 3m from origin X to desired X, reaching an average $V_b$ of 0.39ms$^{-1}$ and $\alpha_b$ of 0.10ms$^{-2}$.

The second test, Experiment II, commanded the robot to move unidirectionally along four desired waypoints (0,1,0), (-2,1,0), (-2,-1,0), and (0,-1,0), which form a square-shaped path. The experiment was repeated three times consecutively. As shown in Fig. 6, an average position error of 0.69m and std of 0.68 are observed. With a shorter distance traveled by the robot, which is at 2m between waypoints, the average $V_b$ and $\alpha_b$ are lower than in Experiment I at 0.27ms$^{-1}$ and 0.06ms$^{-2}$ respectively.

In Experiment III, as shown in Fig. 7.A., a course was set up to evaluate G-ADAM's ground mode function with more complex waypoints and obstacle courses. The assigned waypoints, which formed an L-shaped path, consisted of (1.5,0,0), (0,0,0), (0,1,0), (-1.5,1,0), (-1.5,-1,0), and (1.5,1,0). The experiment was repeated three times consecutively in a loop with waypoint (1.5,0,0) as the starting point. The obstacle course consisted of six main barriers, each with an entryway width as follows: 0.50m, 0.45m, 0.40m, 0.85m, 0.50m, and 1.50m. As shown in Fig. 8.B., G-ADAM showed consistency in position control when comparing actual and desired paths,

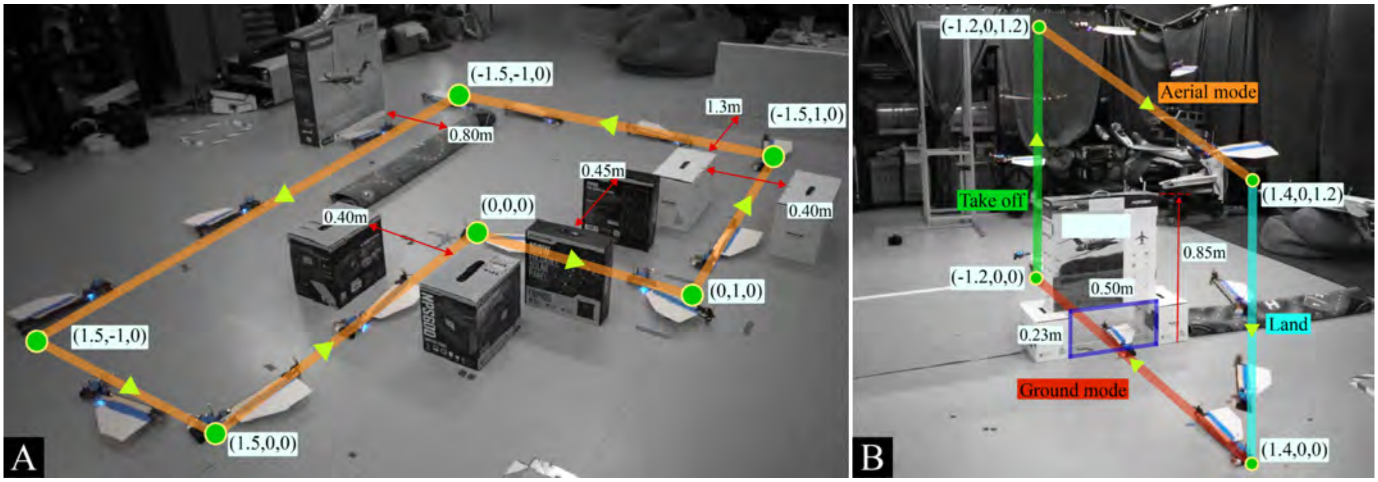


Fig. 7. (A) Experiment III: G-ADAM navigated through an L-shaped obstacle course in ground mode. (B) Experiment VI: G-ADAM started in ground mode, navigated through an obstacle, entered aerial mode, flew over the barrier, landed at the desired waypoint, and repeated.

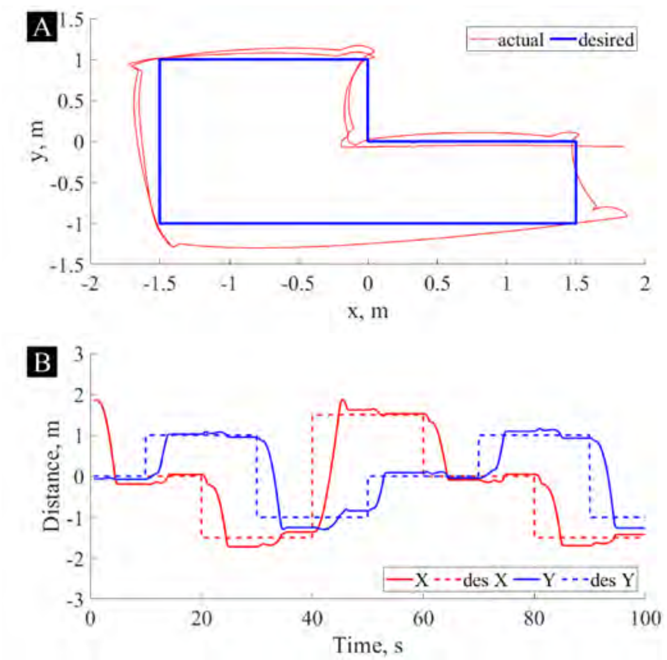


Fig. 8. Experiment III performance: (A) X against Y coordinates between the actual and desired path.

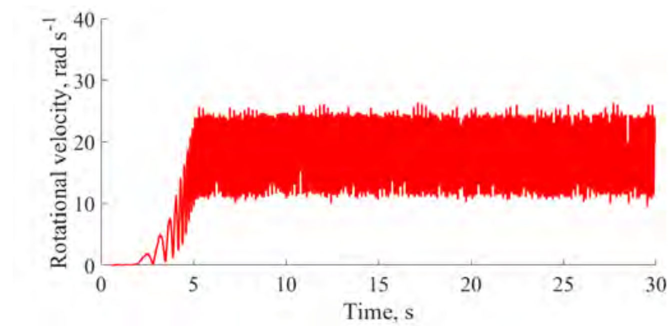


Fig. 9. Experiment IV performance: $\Omega_Z$ against time while hovering.

with a relatively low position error averaging about 0.59 and an std of 0.64. Due to several obstacles and turns, the robot moved at a slower pace compared to the first two experiments, with an average $V_b$ of 0.0.19ms$^{-1}$ and $\alpha_b$ of 0.05ms$^{-2}$.

## B. Aerial Mode Test

In the aerial mode, two experiments were conducted with stabilizer and position controller enabled. Firstly, in Experiment IV, G-ADAM was commanded to hover for 30 seconds with control at a fixed position (0,0,1). The experiment was conducted to evaluate the stability while hovering with position control. Overall, the robot was able to take off and fly consistently with an average position error of 0.01m and an std of 0.09. Also, an average $\Omega_Z$ of 17.80rads$^{-1}$. was achieved. However, as shown in Fig. 9, a high fluctuation of $\Omega_Z$ was observed with an std up to 19.96, which indicated that the robot was trying to maintain stability at the desired hovering position.

The second experiment, Experiment V, was conducted to evaluate G-ADAM's directional control by performing a uni-directional flight along four waypoints: (1,-1,1), (1,1,1.8), (-1,1,1.8), and (-1,-1,1). The experiment was repeated two times consecutively. As shown in Fig. 10.A., the robot performed decently along the four waypoints with a relatively low average position error of 0.01m and std of 0.28. Between each waypoint, the robot had an average $V_b$ of 0.35ms$^{-1}$ and $\Omega_Z$ of 17.43rads$^{-1}$. In Fig. 10.B., the $\Omega_Z$ showed fluctuation with an std of 19.77, which was similar to experiment IV.

## C. Ground-Aerial Transition Mode Test

The final experiment, Experiment VI, was conducted to evaluate the capability of G-ADAM operating both in ground and aerial modes. As shown in Fig. 7.B., barriers were set up with an entryway of 0.50m and 0.23m in length and height, respectively. The maximum height of the barrier was

TABLE II
PERFORMANCE ANALYSIS OF G-ADAM'S EXPERIMENTS

| Parameters | | Experiment | | | | | | Unit |
|---|---|---|---|---|---|---|---|---|
| | | I | II | III | IV | V | VI[b] | |
| Position Error | Mean | 1.58 | 0.69 | 0.59 | 0.01 | 0.01 | 0.25 | m |
| | Std | 1.16 | 0.68 | 0.64 | 0.09 | 0.28 | 0.42 | |
| pwm, Motor | Mean | 1157 | 1110 | 1076 | 1433 | 1450 | 1535; 1531 | |
| | Std | 92.32 | 98.42 | 102.89 | 59.34 | 59.61 | 103.45; 183.42 | |
| Linear Velocity[d], $V_\mathrm{b}$ | Max | 1.43 | 1.55 | 1.37 | - | 2.24 | 1.38; 3.63 | m s$^{-1}$ |
| | Mean | 0.39 | 0.27 | 0.19 | - | 0.35 | 0.23; 0.50 | m s$^{-1}$ |
| | Std | 0.34 | 0.34 | 0.29 | - | 0.25 | 0.29; 0.43 | |
| Linear Acceleration[d], $a_\mathrm{b}$ | Mean | 0.10 | 0.06 | 0.05 | - | 0.14 | 0.07; 0.12 | m s$^{-2}$ |
| | Std | 7.10 | 6.18 | 4.68 | - | 10.25 | 5.81; 21.04 | |
| Rotational Velocity[e], $\Omega_\mathrm{Z}$ | Max | - | - | - | 26.26 | 39.48 | 46.02 | rad s$^{-1}$ |
| | Mean | - | - | - | 17.80 | 17.43 | 13.87 | rad s$^{-1}$ |
| | Std | - | - | - | 19.96 | 19.77 | 16.84 | |

[a] Experiment I: Ground (2 waypoints); II: Ground (4 waypoints); III: Ground (6 waypoints); IV: Aerial (hovering); V: Aerial (4 waypoints); VI: Ground-Aerial.
[b] Parameter Values are in the following order: ground, aerial mode.
[c] In aerial mode, the servo direction is fixed at 90 degrees. Thus, the servo pwm value remains constant.
[d] Experiment VI has linear velocity and acceleration in both modes.
[e] Rotational velocity is only significant and measured in aerial mode, which is applicable to experiment IV, V, and VI.

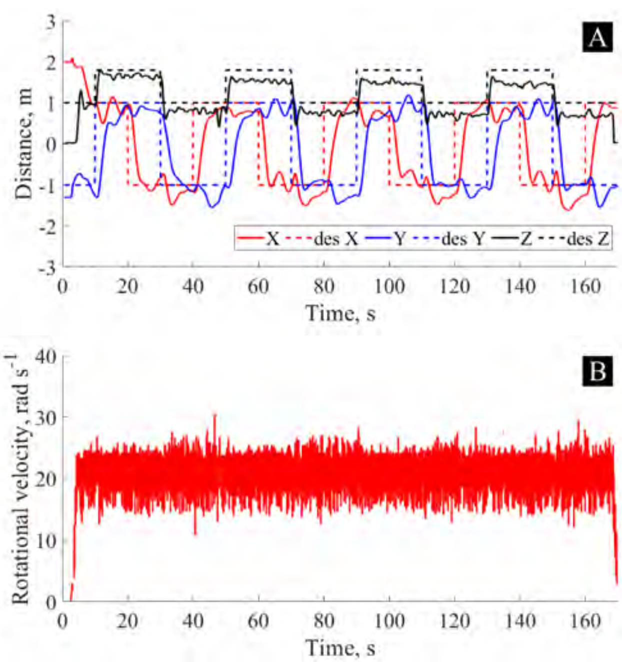


Fig. 10. Experiment V performance: (A) X, Y, and Z coordinates between actual and desired path against time and (B) $\Omega_\mathbf{Z}$ against time during flight between 4 waypoints.

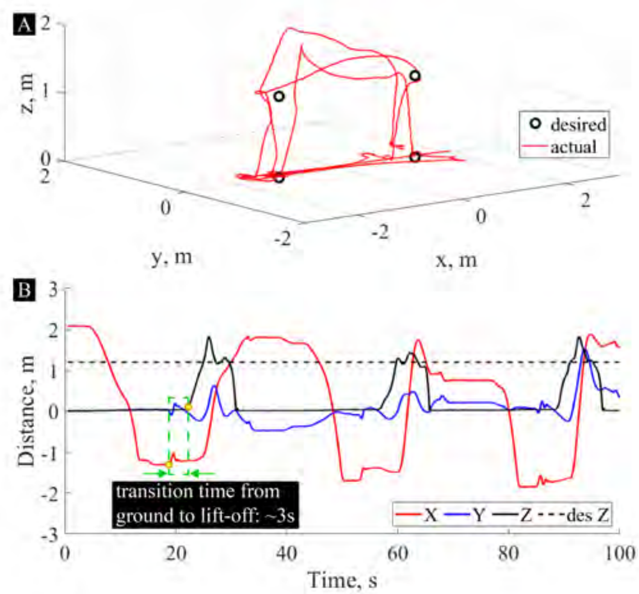


Fig. 11. Experiment VI performance: (A) X, Y, and Z coordinates in 3-D between the actual path and desired waypoints. (B) X, Y, and Z coordinates between the actual and desired path against time. Transition time from ground to lift-off is highlighted.

0.85m, and G-ADAM had to navigate through the entryway and fly over the highest point of the barrier to return to the starting coordinate. The operation involved manual control via transmitter-receiver PPM communication and the stabilizer and position controller. Manual control was used for the ground movement from waypoint (1.4,0,0) to (-1.2,0,0), taking off and landing from waypoint (-1.2,0,0) to (-1.2,0,1.2) and (1.4,0,1.2) to (1.4,0,0) respectively. The stabilizer and position controller was used to fly over the barrier from waypoint (-1.2,0,1.2) to (1.4,0,1.2). Overall, G-ADAM performed well during transition mode regardless of the combination of manual and autonomous control as shown in Fig. 11.A., with an average position error of 0.25m and std of 0.42. The average $V_b$ was 0.23ms$^{-1}$ in ground mode and 0.50ms$^{-1}$ in aerial mode while the $\Omega_\mathbf{Z}$ during flight is 13.87rads$^{-1}$. The experiment showed that G-ADAM could quickly transition between ground and aerial modes, taking approximately 3 seconds to transition from ground mode to lift-off, as highlighted in Fig.

11.B. Other experimental results are presented in Table II.

## CONCLUSION

In conclusion, we present a transformable monocopter with dual actuators capable of moving on the ground and flying in the air on a single platform. By incorporating a servo to control the yaw direction of the motor, G-ADAM can move and change direction to the left and right. Additionally, the transition between ground and aerial modes is relatively direct and quick by turning the motor directly at a fixed angle of 90º to the leading edge direction.

The current G-ADAM prototype also permits autonomous operation utilizing a closed-loop control with motion-capture cameras. The experiment shows G-ADAM's ability to move autonomously on the ground through an obstacle course to desired waypoints with relatively minor position deviation. Due to its rotational freedom on the ground, G-ADAM can recover to desired positions and complete the mission successfully. In the aerial mode test, G-ADAM successfully demonstrates position control in both hovering and flying in a circuit autonomously.

Furthermore, G-ADAM demonstrates the ability to execute a transition mission from ground mode to aerial mode rapidly in 3 seconds in the final experiment. Overall, the experiment highlights the key feature of G-ADAM that enables it to navigate through obstacles on the ground when the flight path is obstructed, and fly over barriers when ground path is unavailable.

## REFERENCES

[1] Y. Ding, B. Xin, and J. Chen, "A Review of Recent Advances in Coordination Between Unmanned Aerial and Ground Vehicles," Unmanned Systems, vol. 09, no. 02, pp. 97–117, Feb. 2021, doi: 10.1142/s2301385021500084.

[2] L. Simon, and G. L. Besnerais, "Issues in Cooperative Air/Ground Robotic Systems," Springer Tracts in Advanced Robotics, 2010, pp. 421–432, doi: 10.1142/S2301385021500084.

[3] B. Hament and P. Oh, "Unmanned aerial and ground vehicle (UAV-UGV) system prototype for civil infrastructure missions," 2018 IEEE International Conference on Consumer Electronics (ICCE), Jan. 2018, doi: 10.1109/ICCE.2018.8326346.

[4] A. Kalantari et al., "Drivocopter: A concept Hybrid Aerial/Ground vehicle for long-endurance mobility," 2020 IEEE Aerospace Conference, Big Sky, MT, USA, 2020, pp. 1-10, doi: 10.1109/AERO47225.2020.9172782.

[5] M. Nir and D. Zarrouk, "Flying STAR, a Hybrid Crawling and Flying Sprawl Tuned Robot." 2019 International Conference on Robotics and Automation (ICRA), May 2019, doi: 10.1109/ICRA.2019.8794260.

[6] K. Tanaka et al., "A design of a small mobile robot with a hybrid locomotion mechanism of wheels and multi-rotors," 2017 IEEE International Conference on Mechatronics and Automation (ICMA), Takamatsu, Japan, 2017, pp. 1503-1508, doi: 10.1109/ICMA.2017.8016039.

[7] Y. Mulgaonkar et al., "The flying monkey: A mesoscale robot that can run, fly, and grasp," 2016 IEEE International Conference on Robotics and Automation (ICRA), Stockholm, Sweden, 2016, pp. 4672-4679, doi: 10.1109/ICRA.2016.7487667.

[8] L. Daler, J. Lecoeur, P. B. Hählen and D. Floreano, "A flying robot with adaptive morphology for multi-modal locomotion," 2013 IEEE/RSJ International Conference on Intelligent Robots and Systems, Tokyo, Japan, 2013, pp. 1361-1366, doi: 10.1109/IROS.2013.6696526.

[9] S. K. H. Win, L. S. T. Win, D. Sufiyan, G. S. Soh and S. Foong, "An Agile Samara-Inspired Single-Actuator Aerial Robot Capable of Autorotation and Diving," in IEEE Transactions on Robotics, vol. 38, no. 2, pp. 1033-1046, April 2022, doi: 10.1109/TRO.2021.3091275.

[10] S. K. H. Win, L. S. T. Win, D. Sufiyan, G. S. Soh and S. Foong, "Dynamics and Control of a Collaborative and Separating Descent of Samara Autorotating Wings," in IEEE Robotics and Automation Letters, vol. 4, no. 3, pp. 3067-3074, July 2019, doi: 10.1109/LRA.2019.2924837.

[11] L. S. T. Win, S. K. H. Win, D. Sufiyan, G. S. Soh and S. Foong, "Achieving Efficient Controlled Flight with A Single Actuator," 2020 IEEE/ASME International Conference on Advanced Intelligent Mechatronics (AIM), Boston, MA, USA, 2020, pp. 1625-1631, doi: 10.1109/AIM43001.2020.9159008.

[12] J. E. Low, L. T. S. Win, D. S. B. Shaiful, C. H. Tan, G. S. Soh and S. Foong, "Design and dynamic analysis of a Transformable Hovering Rotorcraft (THOR)," 2017 IEEE International Conference on Robotics and Automation (ICRA), Singapore, 2017, pp. 6389-6396. doi: 10.1109/ICRA.2017.7989755

[13] H. Bhardwaj, X. Cai, S. K. H. Win, and S. Foong, "Design, Modeling and Control of a Two Flight Mode Capable Single Wing Rotorcraft with Mid-Air Transition Ability." IEEE Robotics and Automation Letters, vol. 7, no. 4, Oct. 2022, pp. 11720–11727, https://doi.org/10.1109/lra.2022.3205454.

[14] X. Cai, S. K. H. Win, L. S. T. Win, D. Sufiyan and S. Foong, "Cooperative Modular Single Actuator Monocopters Capable of Controlled Passive Separation," 2022 International Conference on Robotics and Automation (ICRA), Philadelphia, PA, USA, 2022, pp. 1989-1995, doi: 10.1109/ICRA46639.2022.9812182.

[15] X. Cai, S. K. H. Win, H. Bhardwaj and S. Foong, "Modeling, Control and Implementation of Adaptive Reconfigurable ROtary Wings (ARROWs)," in IEEE/ASME Transactions on Mechatronics, doi: 10.1109/TMECH.2023.3235346.

[16] Y. Liu, J. Wang, Y. Shi, Z. He, F. Liu, W. Kong and Y. He, "Unmanned Airboat Technology and Applications in Environment and Agriculture." Computers and Electronics in Agriculture, vol. 197, June 2022, p. 106920, doi: 10.1016/j.compag.2022.106920.

[17] K. J. Astrom, R. E. Klein and A. Lennartsson, "Bicycle dynamics and control: adapted bicycles for education and research," in IEEE Control Systems Magazine, vol. 25, no. 4, pp. 26-47, Aug. 2005, doi: 10.1109/MCS.2005.1499389.

[18] S. K. H. Win, L. S. T. Win, D. Sufiyan, and S. Foong, "Design and control of the first foldable single-actuator rotary wing micro aerial vehicle," Bioinspiration Biomimetics, vol. 16, no. 6, p. 066019, Nov. 2021, doi: 10.1088/1748-3190/ac253a.